Dynamic and static friction measurements of elastomer footwear blocks on ice surface

Jakobsen, Lasse; Auganaes, Sondre Bergtun; Buene, Audun Formo; Sivebaek, Ion Marius; Klein-Paste, Alex

Published in:
Tribology International

DOI (link to publication from Publisher):
10.1016/j.triboint.2022.108064

Publication date:
2022

Document Version
Publisher's PDF, also known as Version of record

Tribology International 178 (2023) 108064

Contents lists available at ScienceDirect

Tribology International

journal homepage: www.elsevier.com/locate/triboint

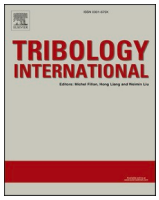

Dynamic and static friction measurements of elastomer footwear blocks on ice surface

Lasse Jakobsen [a,*], Sondre Bergtun Auganaes [b], Audun Formo Buene [b], Ion Marius Sivebaek [a], Alex Klein-Paste [b]

[a] Department of Mechanical Engineering, Technical University of Denmark, Copenhagen, Denmark
[b] Department of Civil and Environmental Engineering, Norwegian University of Science and Technology, Trondheim, Norway

ARTICLE INFO

Keywords:
Footwear
Slip resistance
Elastomer friction
Ice

ABSTRACT

This study conducted friction experiments of three elastomer block materials on ice (low pressure injection of polyurethane (PU), injection moulding of a thermoplastic polyurethane (TPU) and vulcanization of rubber (RU)), with a linear tribometer operating under four different ambient air temperatures (−10 to 0 °C) and six different sliding velocities (0.3–5 m/s). At low temperatures (−10 °C and −5 °C), the RU material showed the highest dynamic and static friction. However, at high temperatures (−2 °C and 0 °C) the PU revealed the highest dynamic friction and highest static friction at 0 °C. We discuss the physical phenomena's of elastomer friction on ice and in relation to the application of footwear slipping on ice.

1. Introduction

Rubber and elastomer friction on ice surfaces is of great importance in relation to skid resistance of winter tires and slip resistance of footwear. The latter can lead to falling and serious injury if insufficient friction between footwear and ice exists [8,19]. In Norway, the most frequent cause of work-related injuries in 2020 was due to falls [45]. This challenge is also present in Denmark, with 110,000 reported fall accidents, where 750 had fatal outcome in 2016 [46]. One of the leading causes of falls is due to slipping [18,20]. In the Scandinavian countries slippery surfaces is a well-known phenomenon, which often implies snow- and ice-covered roads and walkway pavements. This leads to increased risk of slipping and falling for pedestrians and outdoor workers [12,16]. Therefore, it is important to work on potential strategies to increase slip resistance include spreading sand or salt [14]. The latter is especially an effective dissolver of ice and snow [49], which results in increased coefficient of friction between viscoelastic materials and wet pavements [29]. Footwear outsoles are most often constructed of viscoelastic materials, such as polyurethane (PU) [16], natural rubber [16] and thermoplastic polyurethane (TPU) [39], and the choice of outsole material affects the slip resistance on ice [21]. However, research on footwear slipperiness has primarily been aimed at indoor contaminated surfaces ([24,26]; D. [33,52]), where footwear for outdoor occupations has received less attention [4]. Furthermore, it is argued that the most slip resistant footwear materials on contaminated surfaces, may not be the ideal material candidates on icy surfaces [15].

For classification and certification purposes, footwear can be tested on ice surfaces in accordance with testing parameters of the ISO 13287 - Personal protective equipment – Test method for slip resistance (ISO 13287:[43]). One of the testing parameters implies a sliding velocity of 0.3 m/s. However, slipping events starts when the static friction between the shoe and ice is exceeded. After this, the sliding velocity quickly increases and can be as high as 2.5 m/s [9]. This is an important fact, since the friction properties of viscoelastic outsole materials are dependent on temperature and load frequency [37], hence also sliding velocity [25]. Therefore, it is important to conduct static and dynamic friction measurements of viscoelastic materials in a range of sliding velocities and temperatures to obtain realistic application-oriented results. e.g. the tire-ice contact mechanism is an application where the viscoelastic material properties have been found to affect elastomer friction on ice [28] and is thus also expected to affect the somewhat similar contact mechanism between footwear and ice. Thorough studies of rubber [30] and polymer [5] friction on ice, with varying sliding velocities, has been made with both experimental and modelling approaches. However, to the author's knowledge, specific measures performed on elastomer outsole material candidates, during biomechanical relevant loading conditions on ice, has not been reported. Biomechanical loading conditions such as normal load, static contact time and

* Corresponding author.
E-mail address: lasjak@mek.dtu.dk (L. Jakobsen).

https://doi.org/10.1016/j.triboint.2022.108064
Received 21 June 2022; Received in revised form 27 October 2022; Accepted 10 November 2022
Available online 13 November 2022

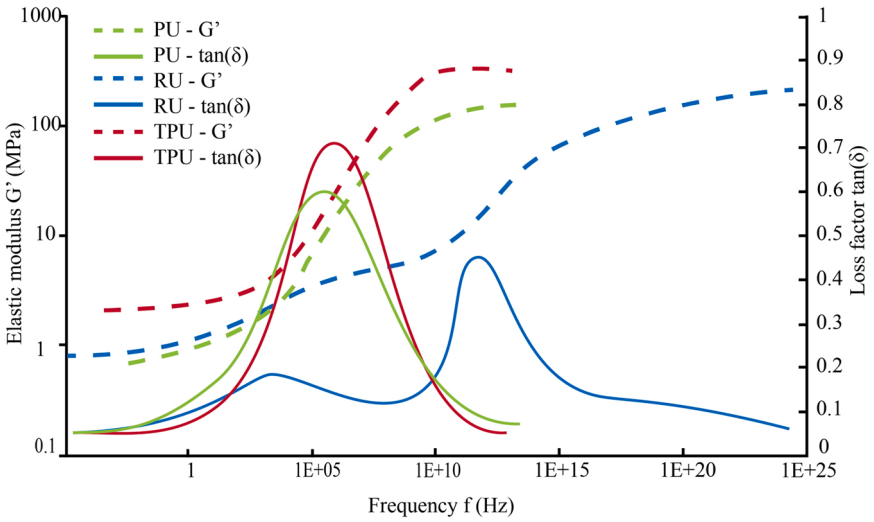

Fig. 1. Master curves for the three materials obtained with dynamic mechanical analysis (T 20 °C).

Table 1
Material properties obtained with dynamic mechanical analysis at selected freezer temperatures.

	-10 °C		-5 °C		-2 °C		0 °C	
	G' (MPa)	tan (δ)	G' (MPa)	tan (δ)	G' (MPa)	tan (δ)	G' (MPa)	tan (δ)
PU	1.9	0.39	1.65	0.29	1.5	0.26	1.4	0.24
TPU	3.1	0.28	2.95	0.195	2.85	0.16	2.8	0.14
RU	2.2	0.16	1.7	0.185	1.4	0.14	1.2	0.12

Table 2
Surface energy measurements. CA(H_2O) = contact angle with distilled water; CA (CH_2Cl_2) = contact angle with diiodomethane; SFE_{tot} = total surface free energy; P/D ratio = polar/dispersive ratio.

Sample	CA (H_2O) [°]	CA (CH_2Cl_2) [°]	SFE^{tot} [mN/m]	P/D ratio
PU	97.39 ± 0.67	91.96 ± 2.05	16.65 ± 1.33	0.41
TPU	94.99 ± 0.07	54.46 ± 1.05	32.70 ± 0.67	0.03
RU	109.19 ± 0.18	91.24 ± 0.56	13.46 ± 0.31	0.11

sliding velocity is referred to as biofidelity, whereas the ability to replicate realistic walkway surfaces and contaminants is referred to as environmental fidelity [8].

To investigate real-world slipping events, it is crucial to acquire footwear slip resistance measurements with actual footwear outsole materials, obtained under bio- and environmental fidelity conditions. This is the motivation to perform controlled indoor tests on a linear tribometer to determine the friction properties between different elastomer materials used for footwear outsoles on an ice surface.

2. Methods

Friction properties between three outsole materials were quantified with a linear tribometer placed in a walk-in freezer. The tribometer is described in details by Giudici and colleagues [17] and evaluated for precision by Auganæs and colleagues [3]. Footwear material properties, ice surface construction and characteristics, and testing procedure are described in the following sections.

2.1. Footwear outsole material samples

The three materials correspond to three different footwear outsole manufacturing processes, namely: low pressure injection of polyurethane (PU), injection moulding of a thermoplastic polyurethane (TPU) and vulcanization of rubber (RU). The materials were provided as material sheets by ECCO (ECCO A/S, Bredebro, Denmark).

2.1.1. Outsole material mechanical characterization

The materials had a short term (< 10 s) shore A hardness of; PU = 56, TPU = 80 and RU = 68. Dynamic material properties were characterized with Dynamic Mechanical Analysis (DMA) using the time-temperature superposition (TTS) principle [34]. Ø8 mm samples of the three materials were cooled to − 130 °C and a thermogram was measured from − 130 °C to ~ 300 °C at 1 Hz and 2 °C/min. Frequency sweeps from 10 to 0.1 Hz are done at selected temperatures. TTS master curves were constructed with 23 °C as the reference temperature and are illustrated in Fig. 1. Material stiffness (G) and damping (tan(δ)) corresponding to the selected freezer temperatures (−10, −5, −2 and 0 °C) are presented in Table 1.

2.1.2. Outsole material surface characterization

The hydrophobicity/wettability of the three materials were identified via surface energy measurements and performed with a Krüss Mobile Surface Analyser (Flexible Liquid) with distilled water (MilliPore) and diiodomethane (Merck). Due to the high density of diiodomethane (3.32 g/cm3) drops of 1 μL were deposited while for water, 1.5 μL drops were analysed. Five measurements were collected per sample and liquid. The surface free energy (SFE) of the rubbers were calculated with the Owens-Wendt-Rabel-Kaelble model by the Krüss ADVANCE software, yielding the total surface free energy (SFE^{tot}) as well as the dispersive and polar contributions. The surface energy properties are presented in Table 2.

Two square blocks (25 ×25 mm) were cut of each of the three materials and glued to 3D printed mounts as illustrated in Fig. 2. The material surface roughness and topography was measured with a non-destructive elastomeric 3D imaging system (GelSight mobile, GelSight, USA), and further analysed using MountainsMap 9.0 software (Digital Surf, France). Roughness parameters (Sa) were calculated according to the ISO 25178 standard [44] with a Robust Gaussian metrological filter of second order (ISO 16610-71) with a cut-off of 2.5 mm. Surface heat map and roughness parameters are presented in Fig. 2.

2.2. Ice surface construction and characterization

The ice surface is presented in Fig. 3 and was created in − 10 °C by building ice layers on top of a 45 mm hard coarse snow layer. Water holding of 0 °C was first sprayed on to create the base and the last layers

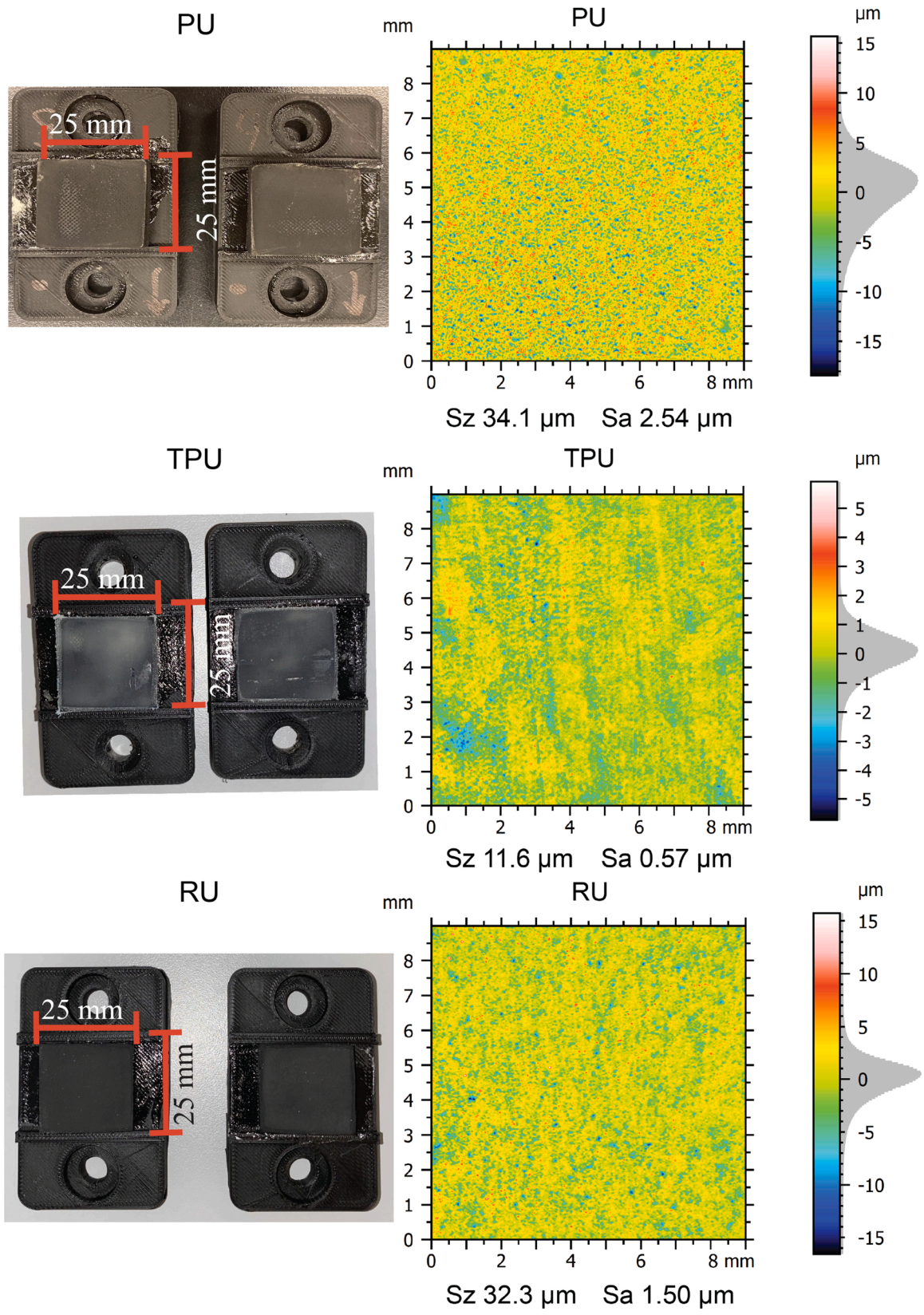

Fig. 2. Visual appearance and surface roughness for the three elastomer material square blocks.

were added with a wet rag and levelled by a squeegee until a smooth ice surface of ~5 mm thickness was reached. Next, the ice surface was thermo-polished with an aluminium box, containing 25 °C water. Ice surface roughness and topography was also characterized with the GelSight 3D imaging system and analysed using MountainsMap 9.0 software.

The ice surface topography is plotted as a heat map (Fig. 4), illustrating the ice surface roughness profile for one sliding track (TPU in

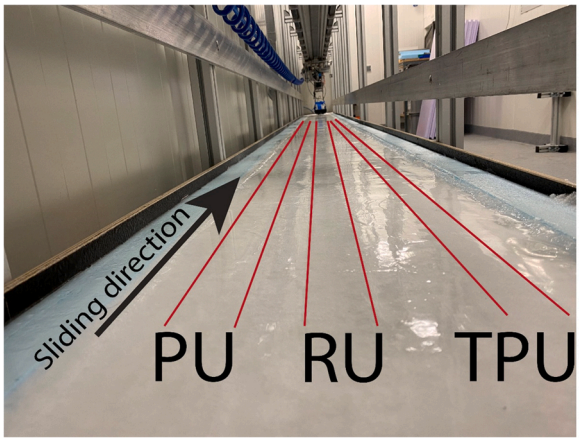

Fig. 3. Photo of the ice surface.

Fig. 3) at 0 °C and − 10 °C before and after friction measurements. At 0 °C the average ice surface roughness (Sa) and peak to valley height (Sz) was 0.93 μm and 26.6 μm respectively, before friction measurements, where Sa = 0.65 μm and Sz = 13 μm after friction measurements. At − 10 °C, Sa = 1.15 μm and Rz = 22 μm before friction measurements, where Sa = 1.17 μm and Rz = 18.9 μm after friction measurements.

2.3. Test procedure for friction measurements

A linear tribometer (illustrated in Fig. 5), located in the Snowlab at the Norwegian University of Science and Technology, was used to determine friction properties between the three outsole materials and the ice surface.

The materials were tested under four different temperatures (−10, −5, −2 and 0 °C). When the temperature was changed, the ice had at least 20 h to acclimatize, before measurements were performed. Before friction measurements, the outsole material specimens were abraded with 400 grit sandpaper (in compliance with the ISO 13287 - Personal protective equipment – Test method for slip resistance (ISO 13287: [43])), cleaned with water and dried with compressed air and then at the ambient temperature corresponding to the freezer temperature for at least 20 h. This cleaning procedure was repeated when the freezer temperature was changed.

Two square material blocks were placed 440 mm (center of one block to center of the other block) on an aluminium profile beam, which acted as the interface between a housing slider and the material blocks (see Fig. 5). This provided a mechanically stabile configuration, compared to measuring on only one slider block, preventing unwanted oscillations when accelerating the slider.

A normal force of 500 N was applied in the middle of the material blocks, thus a corresponding contact pressure of 0.8 MPa was reached. Pressures in the range of 0.2–1 MPa are previously found to be realistic, when determining footwear/surface slip resistance [10]. The three material specimens underwent measurements with six different sliding velocities (0.3, 1, 2, 3, 4, 5 m/s) in a randomized order, for each temperature. Each material specimen had its own sliding track as illustrated in Fig. 3. Thus, the track alignment slider (Fig. 5) was moved laterally when changing materials. Ten run-in measurements for each track were performed for each temperature. Next, five measurements were performed for all sliding velocities, with a custom-made trajectory program. The custom-made trajectory program implied a five-phase program (Fig. 6) consisting of I. slow dynamic sliding (0.1 m/s for 20 cm), II. Resting (500 ms), III. acceleration, IV. target sliding velocity (alteration of the six different sliding velocities) and V. deceleration. Hence, all

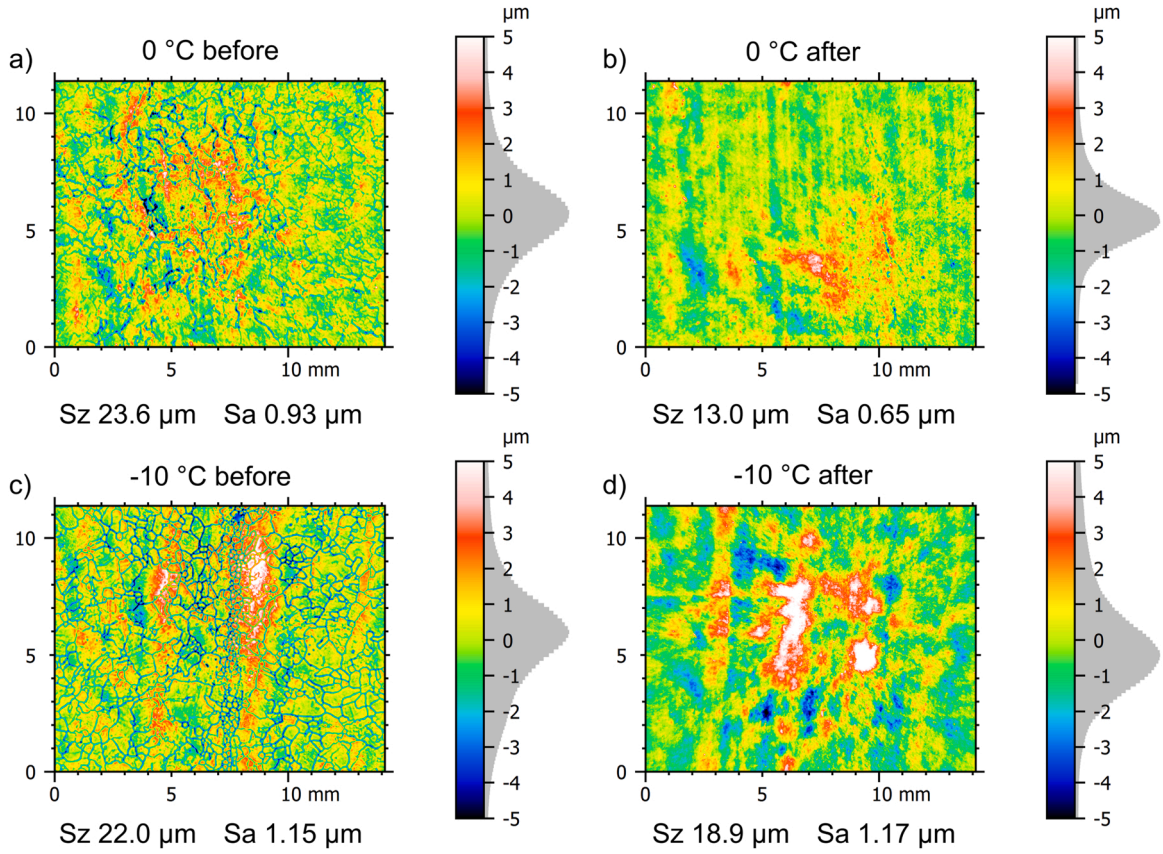

Fig. 4. Topography GelSight images at the same approximate location of one ice track (TPU) surface at 0 °C and − 10 °C before and after friction measurements (n = 40). The image size is 14 * 12 mm, where the forward sliding direction in the images is vertical upwards.

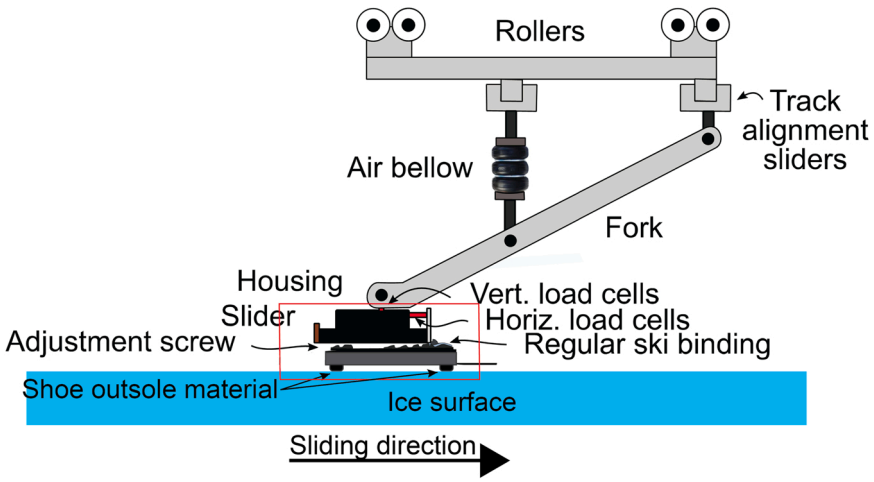

Fig. 5. Illustration of the linear tribometer with shoe outsole material specimen sliding on ice surface. Adapted from [3].

Trajectory program

Step:	I	II	III	IV	V
					
Movement:	Dynamic	Resting for 500 ms	Acceleration	Target velocity	Deceleration
Velocity [m/s]:	0.1	0.0	-	0.3 - 5	-
Elapsed diatance [m]:	0	0.2	0.2 - 1.2	1.2 - 3	3 - 4

Fig. 6. Trajectory program for the tribometer. I. Slow dynamic sliding (0.1 m/s for 20 cm), II. Resting (500 ms), III. Acceleration, IV. Target-sliding velocity (alteration of the six different sliding velocities), V. Deceleration.

phases were consistent between all measurements, except from phase 4, where the sliding velocity was altered.

The sliding velocity of 0.3 m/s and a static contact time of maximum 1000 ms is in compliance with the ISO 13287 (ISO 13287:[43]). 30 s waiting period between each measurement was kept consistent throughout all measurements.

2.4. Data processing

Determination of the coefficient of friction was performed by calculating the arithmetic average of five measurements by dividing the horizontal force with the normal force. The dynamic coefficient of friction is calculated within the measurement region IV (Fig. 6). When determining the static coefficient of friction (SCOF), the peak friction coefficient in the position range of II to III (Fig. 6) was found and averaged for five measurements.

2.5. Friction measurements

An example of the slider trajectory for a typical measurement including I. dynamic movement (0.1 m/s), II. static coefficient of friction, III. acceleration (velocity ramp up), IV. target velocities (0.3 – 5 m/s) and V. deceleration (velocity ramp down) as function of sliding distance, is illustrated in Fig. 7a. The dynamic movement period (see Fig. 6) is identical for all sliding velocities until the resting pause for 500 ms is reached. The target velocity is achieved after 1 m for velocities 1–5 m/s, however for 0.3 m/s the target velocity is achieved after ~0.2 m sliding distance. For sliding velocities 2–5 m/s the actual sliding velocity is slightly lower than the target velocity, which is due to a discrepancy in tribometer motor control. The return velocity is 1 m/s for all measurements. Fig. 7b illustrates the coefficient of friction as function of sliding distance. The SCOF is obtained after step II. (500 ms pause). The average DCOF is measured in the green area, where the sliding velocity is steady.

3. Results

At − 10 °C (Fig. 8) the DCOF tends to decrease with increasing sliding velocity for all three materials. In addition, the velocity dependency is highest at − 10 °C and diminishes as the temperature approaches 0 °C. The RU had the highest DCOF followed by the PU and TPU respectively. At − 5 °C (Fig. 9) the DCOF tends to decrease with increasing sliding velocity for all three materials. The RU still had the highest DCOF from 0.3 to 1 m/s, but from 2 m/s to 5 m/s the PU had the highest DCOF. At − 2 °C (Fig. 10) the DCOF tends to decrease with increasing sliding velocity for RU and TPU. The PU had the highest DCOF among the three materials and tends not to systematically decrease with sliding velocity. At − 0 °C (Fig. 11) the DCOF is less affected by sliding velocity for all three materials, compared to the other temperature measurements. A slight DCOF increase as function of increased sliding velocity appears – most distinctly for the PU.

Averaged static coefficient of friction across all sliding velocities from − 10–0 °C for the three outsole materials are presented in Fig. 12. The RU material reveals the highest SCOF for − 10 °C, − 5 °C and − 2 °C among the three materials. However, at 0 °C the PU material has the highest SCOF followed by TPU and RU respectively.

4. Discussion

At low temperatures (−10 °C and −5 °C) the vulcanized rubber (RU)

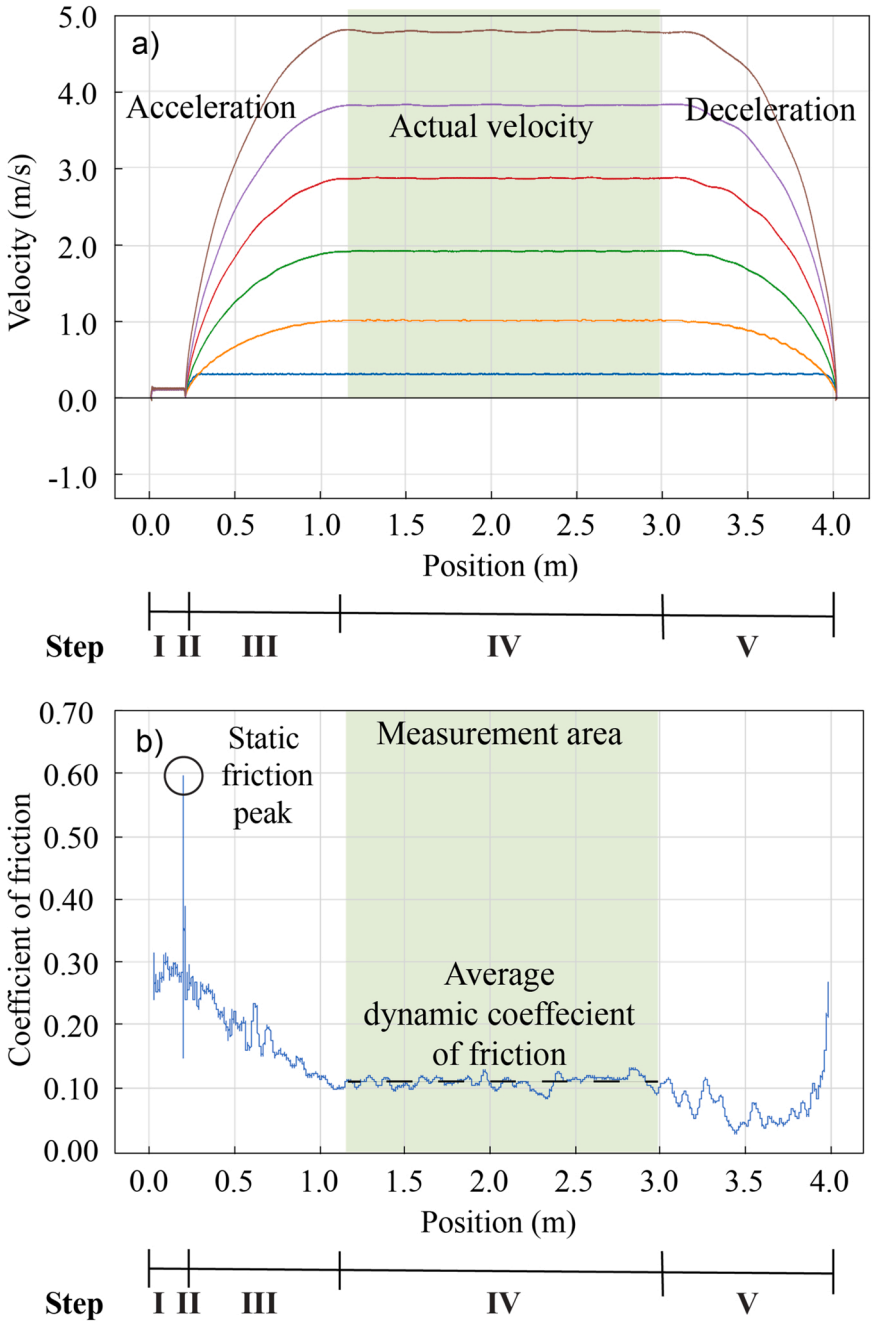

Fig. 7. a: Illustration of the velocity as function of sliding distance (m). White areas illustrates the acceleration and deceleration phases and the green area is the actual velocity. b: Example of static and dynamic friction coefficient as function of sliding distance. Green area illustrates the measurement area for dynamic coefficient of friction. The dashed line is the average DCOF. The example is one measurement for RU at − 5 °C with a sliding velocity of 4 m/s.

showed the highest dynamic friction coefficients at sliding velocities from 0 to 2 m/s, compared to the injection moulded thermoplastic polyurethane (TPU) and the low pressure injected polyurethane (PU). At low temperatures and at sliding velocities from 2 to 5 m/s, the PU showed the highest DCOF. At high temperatures (−2 °C and 0 °C) the PU showed the highest dynamic friction coefficients compared to the TPU and RU materials. At 0 °C, the PU revealed much higher SCOF compared to the TPU and RU materials.

4.1. Elastomer block friction on ice

The observed velocity dependencies in our study are in line with previous research of rubber friction on ice, where DCOF decreased with increased temperatures [13,30,41] and increased with sliding velocity [30,41,48]. The decrease in DCOF, as function of increased sliding velocity and increased ambient temperature, is likely due to an increase in meltwater film formation, which separates the elastomer and ice surfaces and acts as a lubrication [30]. At low temperatures, the ice surface is solid-like and the surface is slightly rougher compared to high temperatures. At this solid-like state, the elastomer elastic modulus supposedly has an important role, since a softer material will more easily comply with the roughness of the substrate and thereby increase the friction. Based on the DMA, the RU material has the lowest elastic modulus at high frequencies (E5-E15 Hz). Hence, when the RU slides at 0.3 m/s at − 10 C° and − 5 C°, it may exhibit vibrations in the range of E5-E15 Hz and this can possibly explain the higher friction at this sliding

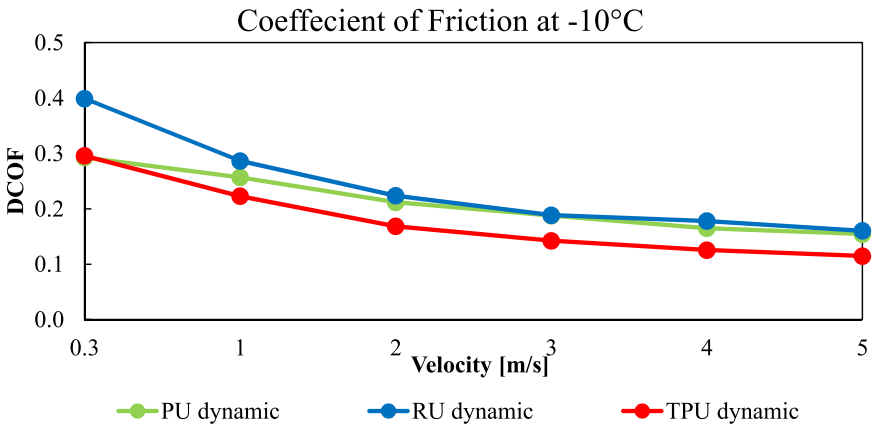

Fig. 8. Average dynamic coefficient of friction (DCOF) at − 10 °C as function of sliding velocity. Error bars with ± standard deviations < 0.02 are not visual and left out.

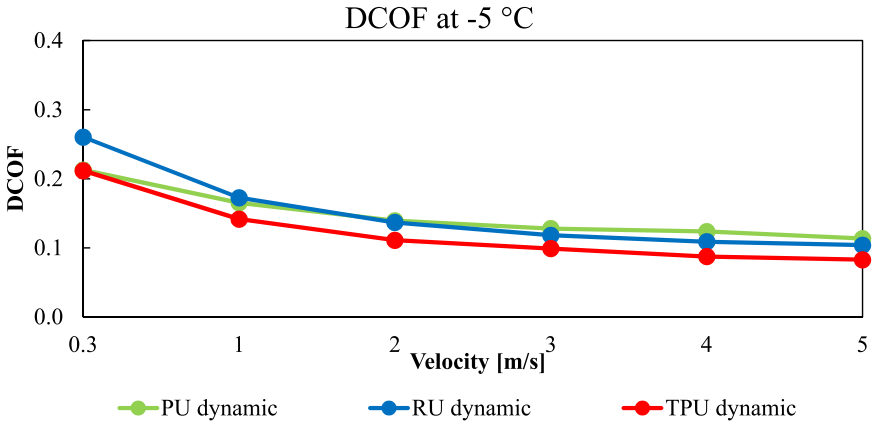

Fig. 9. Average dynamic coefficient of friction (DCOF) at − 5 °C as function of sliding velocity. Error bars with ± standard deviations < 0.02 are not visual and left out.

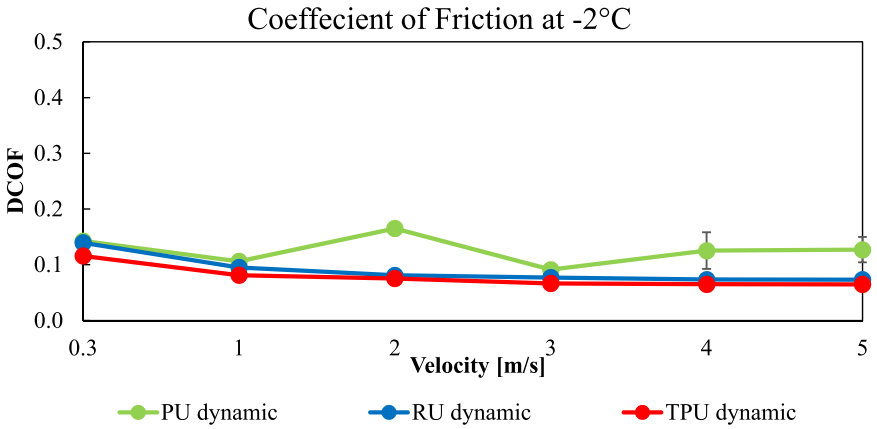

Fig. 10. Average dynamic coefficient of friction (DCOF) at − 2 °C as function of sliding velocity. Error bars with ± standard deviations < 0.02 are not visual and left out.

velocity and temperatures. The damping property (tan(δ)) shown in Fig. 1 has also been linked to the coefficient of friction [37] and tan(δ) is higher for RU at high frequencies than for the other materials. The effect could be more pronounced due the low temperatures, which shift the frequency curve to the left in Fig. 1.

In addition, it is more difficult to generate sufficient meltwater through frictional heating at low temperatures. This is supported by the roughness measurements in Fig. 4, where the polishing of the ice surface is more pronounced at high temperatures. While this can be explained by both temperature-dependent differences in lubrication mechanism and increased ice abrasion due to reduced hardness of warm ice, we are of the opinion this difference in roughness is caused by the different lubrication regimes at 0 °C and − 10 °C. The reason is that more heat is needed to heat the ice to its melting point and the conductive heat fluxes into the ice and the elastomer slider are larger since the temperature gradients are larger [36]. This leaves less heat to generate a water film at

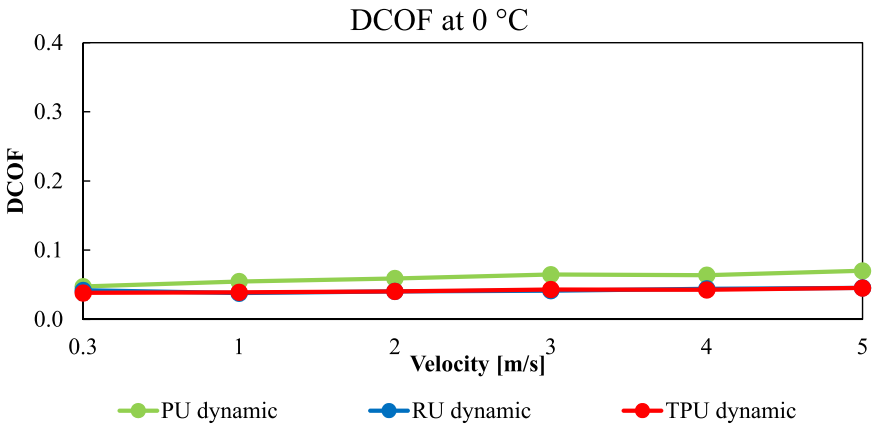

Fig. 11. Average dynamic coefficient of friction (DCOF) at 0 °C as function of sliding velocity. NOTE – RU and TPU are close related and the TPU curve somewhat overshadows the RU curve. Error bars with ± standard deviations < 0.02 are not visual and left out.

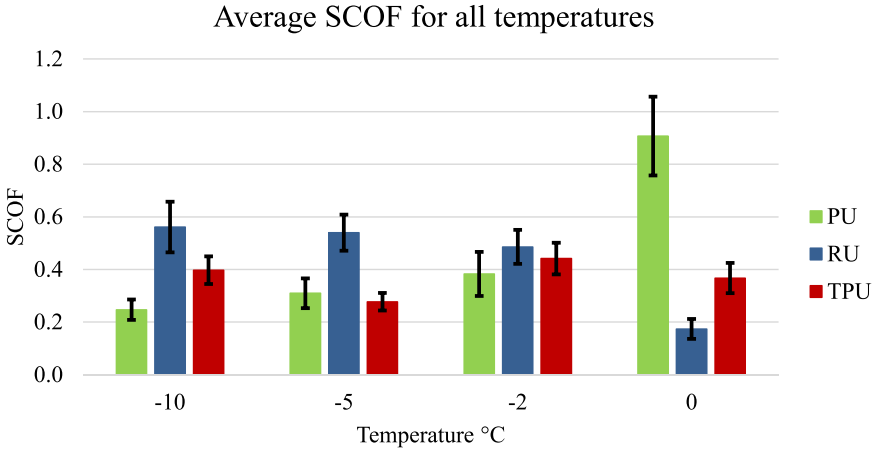

Fig. 12. Average static coefficient of friction (SCOF) for all temperatures (0 °C to −10 °C). Average is taken for all 30 measurements conducted for each temperature. Hence, the acceleration varies as illustrated in Fig. 7A. Error bars represents ± standard deviation.

Table 3
Average dynamic coefficient of friction (DCOF) and static coefficient of friction (SCOF) ± standard deviation at − 10 °C.

-10 °C							
Average COF	Material	0.3 m/s	1 m/s	2 m/s	3 m/s	4 m/s	5 m/s
Dynamic	PU	0.292 ± 0.0008	0.257 ± 0.00014	0.212 ± 0.0016	0.188 ± 0.0031	0.165 ± 0.0005	0.154 ± 0.0014
	RU	0.399 ± 0.0027	0.286 ± 0.0034	0.224 ± 0.0023	0.189 ± 0.0004	0.178 ± 0.0007	0.160 ± 0.0008
	TPU	0.296 ± 0.011	0.223 ± 0.0018	0.168 ± 0.0018	0.142 ± 0.0005	0.126 ± 0.00017	0.115 ± 0.0011
Static	PU	0.216 ± 0.0055	0.198 ± 0.0045	0.223 ± 0.005	0.254 ± 0.0055	0.284 ± 0.0055	0.308 ± 0.0084
	RU	0.694 ± 0.0312	0.427 ± 0.0159	0.443 ± 0.0237	0.582 ± 0.0256	0.625 ± 0.0755	0.596 ± 0.0400
	TPU	0.451 ± 0.0211	0.313 ± 0.0256	0.439 ± 0.0182	0.338 ± 0.0043	0.410 ± 0.0429	0.432 ± 0.0395

Table 4
Average dynamic coefficient of friction (DCOF) and static coefficient of friction (SCOF) ± standard deviation at − 5 °C.

-5 °C							
Average COF	Material	0.3 m/s	1 m/s	2 m/s	3 m/s	4 m/s	5 m/s
Dynamic	PU	0.213 ± 0.005	0.165 ± 0.001	0.139 ± 0.000	0.128 ± 0.0183	0.124 ± 0.002	0.113 ± 0.000
	RU	0.260 ± 0.002	0.173 ± 0.000	0.137 ± 0.000	0.118 ± 0.0006	0.109 ± 0.000	0.104 ± 0.000
	TPU	0.212 ± 0.000	0.142 ± 0.000	0.111 ± 0.000	0.099 ± 0.000	0.087 ± 0.000	0.082 ± 0.001
Static	PU	0.286 ± 0.015	0.243 ± 0.018	0.255 ± 0.0124	0.310 ± 0.018	0.401 ± 0.017	0.363 ± 0.012
	RU	0.521 ± 0.009	0.4201 ± 0.009	0.498 ± 0.049	0.574 ± 0.004	0.622 ± 0.015	0.604 ± 0.012
	TPU	0.271 ± 0.009	0.226 ± 0.013	0.245 ± 0.008	0.313 ± 0.020	0.294 ± 0.015	0.315 ± 0.013

Table 5
Average dynamic coefficient of friction (DCOF) and static coefficient of friction (SCOF) ± standard deviation at − 2 °C.

-2 °C							
Average COF	Material	0.3 m/s	1 m/s	2 m/s	3 m/s	4 m/s	5 m/s
Dynamic	PU	0.143 ± 0.001	0.106 ± 0.001	0.165 ± 0.008	0.091 ± 0.001	0.125 ± 0.033	0.127 ± 0.023
	RU	0.134 ± 0.001	0.095 ± 0.000	0.081 ± 0.000	0.077 ± 0.000	0.074 ± 0.000	0.073 ± 0.000
	TPU	0.116 ± 0.003	0.081 ± 0.000	0.075 ± 0.000	0.067 ± 0.000	0.065 ± 0.000	0.065 ± 0.000
Static	PU	0.348 ± 0.009	0.318 ± 0.011	0.250 ± 0.011	0.444 ± 0.005	0.457 ± 0.057	0.482 ± 0.048
	RU	0.475 ± 0.005	0.389 ± 0.004	0.428 ± 0.005	0.517 ± 0.018	0.519 ± 0.006	0.587 ± 0.008
	TPU	0.412 ± 0.010	0.364 ± 0.01	0.422 ± 0.018	0.424 ± 0.011	0.472 ± 0.008	0.557 ± 0.014

Table 6
Average dynamic coefficient of friction (DCOF) and static coefficient of friction (SCOF) ± standard deviation at 0 °C.

0 °C							
Average COF	Material	0.3 m/s	1 m/s	2 m/s	3 m/s	4 m/s	5 m/s
Dynamic	PU	0.048 ± 0.000	0.055 ± 0.000	0.059 ± 0.000	0.065 ± 0.000	0.064 ± 0.000	0.070 ± 0.000
	RU	0.042 ± 0.000	0.038 ± 0.000	0.041 ± 0.000	0.042 ± 0.000	0.044 ± 0.000	0.046 ± 0.000
	TPU	0.038 ± 0.000	0.039 ± 0.005	0.040 ± 0.000	0.043 ± 0.000	0.043 ± 0.000	0.045 ± 0.000
Static	PU	0.730 ± 0.021	0.744 ± 0.008	0.871 ± 0.005	0.899 ± 0.028	1.083 ± 0.005	1.116 ± 0.011
	RU	0.157 ± 0.004	0.116 ± 0.004	0.155 ± 0.005	0.173 ± 0.004	0.218 ± 0.004	0.226 ± 0.005
	TPU	0.322 ± 0.007	0.291 ± 0.005	0.336 ± 0.011	0.380 ± 0.006	0.412 ± 0.006	0.462 ± 0.015

low temperatures. At high temperatures and high sliding velocities above 1 m/s, the formation of meltwater is likely to increase [42] and makes the elastomer elastic modulus less important. In this stage, friction is mainly determined by the shearing of the meltwater film and the DCOF does not differ much among the three materials. Nonetheless, at 0 °C the effect of sliding velocity tends to change and cause an increase in DCOF as function of increased sliding velocity. This increase in friction at high ice temperatures is likely caused by capillary suction, where the increase in surface meltwater film thickness can cause bridging of water between contact points, which are not load carrying and can cause an increased friction force [11]. PU is a porous material and it is likely that there will be more of such possible bridge contact points and therefore a higher capillary drag, compared to the other two materials.

The SCOF for PU at 0 °C is distinctly higher compared to the RU and TPU material. The porous PU material has the ability to absorb a small amount of water. Therefore, at 0 °C it is likely that the PU absorbs water from the surface melt water film, during the resting period of 500 ms (see Fig. 6 II) and forms ice sintering between the ice surface and the PU surface pores. Furthermore, the PU has a slightly higher surface roughness compared to the other materials and a greater amount of encapsulated melt water may be present. Hence, breaking the ice bonding at stage III (Fig. 6) are likely causing the pronounced SCOF for PU at 0 °C. In addition, the RU has lowest wettability (109.19 ± 0.18° - see Table 2) and therefore is the most hydrophobic material used in this study. At temperatures close to the melting point, increased slider surface hydrophobicity decreases ice friction [27] and thus may contribute to the low SCOF at 0 °C for RU.

4.2. Footwear slip resistance on ice

Rubber outsoles being more slip resistant than PU outsoles at low temperatures is in line with previous research of footwear slip resistance on ice [15]. The research from Gao and colleagues showed that polyurethane outsoles did not perform better than synthetic rubber, nitrile rubber and natural rubber on pure cold ice (−12 °C). They did however not test at high temperatures closer to zero, where we in the present study, found an opposite tendency, revealing higher dynamic friction for PU soles between − 2 and 0 °C and much higher static friction at 0 °C compared to rubber. It should be mentioned, that the exact material compositions for outsoles plays an important role in relation to footwear slip resistance [32] and material properties from the present study may differ from the study by [15].

For the application of footwear slip resistance, sliding velocities above 1 m/s may occur [9,10]. Hence, sliding velocities between 0.5 and 2.5 m/s are probably most relevant in relation to real life slipping accidents. Furthermore, dynamic friction coefficients in the range of 0.1–0.3 is likely to cause slipping [20]. Therefore, temperatures above − 10 °C is likely to cause slipping for the three materials investigated in this study. While the DCOF at 0 °C is low for all three materials, it is worth noticing, that the PU showed highest DCOF and considerably higher SCOF compared to the TPU and RU. This is in line with another study conducted on whole footwear constructed of the same three materials, where it was found that the PU outsole revealed higher DCOF on glycerine/canola oil contaminated steel and tile surfaces, compared to the TPU and RU outsoles [24].

Both SCOF and DCOF are arguably important and the best frictional measure for preventing slipping is under debate [47,50]. A high SCOF may prevent slip initiation when a surface is known/expected to be slippery, since walking subjects tend to reduce their heel velocity when anticipating slippery floors [7]. However, biomechanical studies have demonstrated that if a slip event is initiated, the shoe does not stop sliding [1,23]. In prolongation, the available DCOF magnitude is previously found to be related to the probability of slip events [6,20,22]. Hence, both SCOF and DCOF is suggested to be evaluated, when determining footwear slip resistance [53]. Since the necessary breaking friction force from static to dynamic friction is higher for the PU outsole material at high (close to 0 °C) temperatures compared to TPU and RU, the PU sole may arguably resist the initiation of the dynamic sliding phase. However, due to the low DCOF values at high temperatures the slip probability may still be high. This suggests that one outsole material may not have superior slip resistance on all ice conditions. At low temperatures (−10 °C and - 5 °C) vulcanized rubber may be the better choice, whereas at high temperatures (−2 °C and 0 °C) PU may be a better choice. Recent research have identified that embedding fibers [2,38] in elastomer material enhances friction on icy surfaces. Hence, it can be speculated whether a hybrid outsole construction provides a better slip resistance on ice over a wider temperature range. In fact, a hybrid surface pattern outsole for preventing slips on icy surfaces, has already been made with smooth and rough outsole surface pattern [51] and with hybrid composite materials [40].

Further studies should potentially aim for investigating hybrid outsole constructions, which combines outsole design concepts, outsole materials and composites to accommodate slip resistance over a wider range of ice surface types and temperatures.

4.3. Limitations

This study has some limitations, which should be noted. Despite the fact that the trajectory program for the tribometer included biofidelic testing parameters, it should be noted, that this study lacks validation of human factors. Hence, human specific parameters like e.g. foot motion, normal force build up rate and slip anticipation was not possible to replicate in this study. Furthermore, this study was conducted with elastomer block samples and thus not a realistic reproduction of a common footwear outsole. Outsoles often have more complex geometries, in terms of heel bevelling, outsole pattern and midsole cushioning, which previously has been found to affect the slip resistance [31,35,52]. Lastly, numerous material combinations of RU, PU and TPU may exist and it is not known, whether other material combination may reveal different friction properties. Hence, extrapolation of the findings from this study to other combinations of the materials should be done with caution.

5. Conclusion

This study compared friction of three elastomer block materials (low pressure injection of polyurethane (PU), injection moulding of a thermoplastic polyurethane (TPU) and vulcanization of rubber (RU)), conducted on a linear tribometer operating under four different ambient air temperatures (−10 to 0 °C) and six different sliding velocities (0.3–5 m/s). A custom-made trajectory program for the tribometer enabled the ability to determine dynamic and static friction coefficients and mimic biofidelic testing parameters relevant for slipping. At low (temperatures −10 °C and −5 °C), the RU material had highest dynamic and static friction. However, at high temperatures (−2 °C and 0 °C) the PU showed highest dynamic friction and higher static friction at 0 °C. The high friction for RU at low temperatures could be explained by the low elastic modulus at high frequencies, making the material comply more with the ice surface during specific sliding velocities, compared with the other materials. The high dynamic and static friction for PU at high temperatures could be explained by its porous nature. Based on these findings we suggest further studies of elastomer friction on ice focused on a hybrid construction based on different materials, design concepts and composite solutions, to potentially accommodate slip resistance over a wider temperature range.

Statement of originality

As the corresponding author, I certify that this manuscript is original and its publication does not infringe any copyright. As the corresponding author, I declare that the manuscript has not been previously published, in whole or in part in any other journal or scientific publishing company. In addition, the manuscript does not participate in any other publishing process. As the corresponding author, I declare that all persons listed hereafter were committed in the creation of the paper and were informed about their participation.

Declaration of Competing Interest

The authors declare that they have no known competing financial interests or personal relationships that could have appeared to influence the work reported in this paper.

Data availability

Data will be made available on request.

Acknowledgements

This study was funded by the Danish Working Environment Research Fund (grant number: 20195100816). ECCO Shoes A/S provided the material samples used in this study, but had no role in the interpretation and presentation of the results. The authors want to thank Sophia Sachse from ECCO A/S for her extensive help and very fast execution. Lastly, we want to thank Jesper Bøgelund, Senior R&D Engineer at DDS (device delivery & solutions) at Novo Nordisk for providing the DMA measurements.

Appendix

See Tables 3–6.

.

References

[1] Albert D, Moyer B, Beschorner KE. Three-dimensional shoe kinematics during unexpected slips: implications for shoe–floor friction testing. IISE Trans Occup Ergon Hum Factors 2017;5(1):1–11. https://doi.org/10.1080/21577323.2016.1241963.
[2] Anwer A, Bagheri ZS, Fernie G, Dutta T, Naguib HE. Evolution of the coefficient of friction with surface wear for advanced surface textured composites. Adv Mater Interfaces 2017;4(6). https://doi.org/10.1002/admi.201600983.
[3] Auganæs SB, Buene AF, Klein-Paste A. Laboratory testing of cross-country skis – Investigating tribometer precision on laboratory-grown dendritic snow. Tribol Int 2022;168. https://doi.org/10.1016/j.triboint.2022.107451.
[4] Bagheri ZS, Beltran JD, Holyoke P, Dutta T. Reducing fall risk for home care workers with slip resistant winter footwear. Appl Ergon 2021:*90*. https://doi.org/10.1016/j.apergo.2020.103230.
[5] Bäurle L, Kaempfer TU, Szabó D, Spencer ND. Sliding friction of polyethylene on snow and ice: contact area and modeling. Cold Reg Sci Technol 2007;47(3). https://doi.org/10.1016/j.coldregions.2006.10.005.
[6] Burnfield JM, Powers CM. Prediction of slips: an evaluation of utilized coefficient of friction and available slip resistance. Ergonomics 2006;49(10):982–95. https://doi.org/10.1080/00140130600665687.
[7] Cham R, Redfern MS. Changes in gait when anticipating slippery floors. Gait Posture 2002;15(2):159–71. https://doi.org/10.1016/S0966-6362(01)00150-3.
[8] Chang W-R, Courtney TK, Grönqvist R, Redfern M. Measuring slipperiness—discussions on the state of the art and future research. In: Measuring slipperiness. Taylor & Francis,; 2010. p. 165–72. https://doi.org/10.4324/9780203301913_chapter_8.
[9] Chang W, Grönqvist R, Leclercq S, Brungraber RJ, Mattke U, Strandberg L, et al. The role of friction in the measurement of slipperiness, Part 2: survey of friction measurement devices. Ergonomics 2001;44(13):1233–61. https://doi.org/10.1080/00140130110085583.
[10] Chang W, Grönqvist R, Leclercq S, Myung R, Makkonen L, Strandberg L, et al. The role of friction in the measurement of slipperiness, Part 1: friction mechanisms and definition of test conditions The role of friction in the measurement of slipperiness, Part 1: friction mechanisms and definition of test conditions. Ergonomics 2001;44(13). https://doi.org/10.1080/00140130110085574.
[11] Colbeck, S.C.1992. A review of the processes that control snow friction. Cold Regions Research and Engineering Laboratory, CRREL Monograph, April.
[12] Courtney TK, Sorock GS, Manning DP, Collins JW, Holbein-Jenny MA. Occupational slip, trip, and fall-related injuries can the contribution of slipperiness be isolated? Ergonomics 2001;44(13):1118–37. https://doi.org/10.1080/00140130110085538.
[13] Fulop T, Isitman NA. Frictional characteristics of rubber on ice. Rubber World 2020;262:6.
[14] Gao C, Abeysekera J. The assessment of the integration of slip resistance, thermal insulation and wearability of footwear on icy surfaces. Saf Sci 2002;40(7–8). https://doi.org/10.1016/S0925-7535(01)00062-5.
[15] Gao C, Abeysekera J, Hirvonen M, Grönqvist R. Slip resistant properties of footwear on ice. Ergonomics 2004;47(6). https://doi.org/10.1080/00140130410001658673.
[16] Gauvin, C., Pearsall, D., Damavandi, M., Michaud-Paquette, Y., Farbos, B., Imbeau, D. 2015. Risk factors for slip accidents among police officers and school crossing guards. Available from: ⟨www.csst.qc.ca/AbonnementPAT⟩.
[17] Giudici H, Dahl Fenre M, Klein-Paste A, Rekilä K-P. A technical description of LARS and Lumi: two apparatus for studying tire-pavement interactions. Routes/Roads Mag 2017:49–54.
[18] Grönqvist R, Chang W, Courtney TK, Leamon TB, Redfern MS, K T, et al. Measurement of slipperiness: fundamental concepts and definitions. Ergonomics 2001;44(13):1117. https://doi.org/10.1080/0014013011008552.
[19] Grönqvist R, Hirvonen M. Slipperiness of footwear and mechanisms of walking friction on icy surfaces. Int J Ind Ergon 1995;16(3). https://doi.org/10.1016/0169-8141(94)00095-K.
[20] Hanson JP, Redfern MS, Mazumdar M. Predicting slips and falls considering required and available friction. Ergonomics 1999;42(12):1619–33. https://doi.org/10.1080/001401399184712.
[21] Hsu J, Shaw R, Novak A, Li Y, Ormerod M, Newton R, et al. Slip resistance of winter footwear on snow and ice measured using maximum achievable incline. Ergonomics 2016;59(5):717–28. https://doi.org/10.1080/00140139.2015.1084051.

[22] Iraqi A, Cham R, Redfern MS, Beschorner KE. Coefficient of friction testing parameters influence the prediction of human slips. Appl Ergon 2018;70:118–26. https://doi.org/10.1016/j.apergo.2018.02.017.
[23] Iraqi A, Cham R, Redfern MS, Vidic NS, Beschorner KE. Kinematics and kinetics of the shoe during human slips. J Biomech J 2018;74:57–63. https://doi.org/10.1016/j.jbiomech.2018.04.018.
[24] Jakobsen L, Lysdal, Gertz F, Bagehorn T, Kersting U, Sivebaek, et al. The effect of footwear outsole material on slip resistance on dry and contaminated surfaces with geometrically controlled outsoles. Ergonomics 2022. https://doi.org/10.1080/00140139.2022.2081364.
[25] Jakobsen L, Lysdal FG, Sivebaek IM. Dynamic mechanical analysis as a predictor for slip resistance and traction in footwear. Footwear Sci 2021;13(S1):S57–8. https://doi.org/10.1080/19424280.2021.1917680.
[26] Jones T, Iraqi A, Beschorner K. Performance testing of work shoes labeled as slip resistant. Appl Ergon 2018;68:304–12. https://doi.org/10.1016/j.apergo.2017.12.008.
[27] Kietzig AM, Hatzikiriakos SG, Englezos P. Ice friction: the effects of surface roughness, structure, and hydrophobicity. J Appl Phys 2009;106(2). https://doi.org/10.1063/1.3173346.
[28] Klapproth C, Kessel TM, Wiese K, Wies B. An advanced viscous model for rubber-ice-friction. Tribol Int 2016:*99*. https://doi.org/10.1016/j.triboint.2015.09.012.
[29] Klein-Paste A, Wåhlin J. Wet pavement anti-icing - a physical mechanism. Cold Reg Sci Technol 2013:*96*. https://doi.org/10.1016/j.coldregions.2013.09.002.
[30] Lahayne O, Pichler B, Reihsner R, Eberhardsteiner J, Suh J, Kim D, et al. Rubber friction on ice: experiments and modeling. Tribol Lett 2016;62(2). https://doi.org/10.1007/s11249-016-0665-z.
[31] Lloyd D, Stevenson MG. Measurement of slip resistance of shoes on floor surfaces. Part 2: effect of a bevelled heel. J Occup Health Saf Aust NZ 1989;5:3.
[32] Manning DP, Jones C. The superior slip-resistance of footwear soling compound T66/103. Saf Sci 1994;18(1). https://doi.org/10.1016/0925-7535(94)90040-X.
[33] Manning D, Jones C, Bruce M. Boots for oily surfaces. Ergonomics 1985;28(7):1011–9. https://doi.org/10.1080/00140138508963223.
[34] Menard K, Menard N. Dynamic mechanical analysis. 3rd ed. CRC Press; 2020. https://doi.org/10.1007/978-3-540-29805-2_1224.
[35] Moriyasu K, Nishiwaki T, Shibata K, Yamaguchi T, Hokkirigawa K. Friction control of a resin foam/rubber laminated block material. Tribol Int 2019:*136*. https://doi.org/10.1016/j.triboint.2019.04.024.
[36] Oksanen P, Keinonen J. The mechanism of friction of ice. Wear 1982;78(3). https://doi.org/10.1016/0043-1648(82)90242-3.
[37] Persson BNJ. Theory of rubber friction and contact mechanics. J Chem Phys 2001. https://doi.org/10.1063/1.1388626.
[38] Rizvi R, Naguib H, Fernie G, Dutta T. High friction on ice provided by elastomeric fiber composites with textured surfaces. Appl Phys Lett 2015;106(11). https://doi.org/10.1063/1.4913676.
[39] Sato S, Yamaguchi T, Shibata K, Nishi T, Moriyasu K, Harano K, et al. Dry sliding friction and Wear behavior of thermoplastic polyurethane against abrasive paper. Biotribology 2020:*23*. https://doi.org/10.1016/j.biotri.2020.100130.
[40] Shaghayegh Bagheri Z, Anwer A, Fernie G, Naguib HE, Dutta T. Effects of multi-functional surface-texturing on the ice friction and abrasion characteristics of hybrid composite materials for footwear. Wear 2019:*418–9*. https://doi.org/10.1016/j.wear.2018.11.030.
[41] Skouvaklis G, Blackford JR, Koutsos V. Friction of rubber on ice: a new machine, influence of rubber properties and sliding parameters. Tribol Int 2012:*49*. https://doi.org/10.1016/j.triboint.2011.12.015.
[42] Southern E, Walker RW. Friction of rubber on ice. Nat Phys Sci 1972;237(78). https://doi.org/10.1038/physci237142a0.
[43] Standard, I.2019. Personal protective equipment – footwear – test method for slip resistance (ISO 13287:2019).
[44] Standard, I.2021. Geometrical product specifications (GPS) – surface texture: areal – part 2: terms, definitions and surface texture parameters: DS/ISO 25178-2:2021.
[45] Statistics Norway. Fall vanligste arbeidsulykke; 2021. Available from: ⟨https://www.ssb.no/helse/helseforhold-og-levevaner/statistikk/arbeidsulykker/artikler/fall-vanligste-arbeidsulykke⟩.
[46] Sundhedsstyrelsen. 2016. Sygdomsbyrden i Danmark, Ulykker, Selvskade og Selvmord 2016. Available from: ⟨www.sst.dk⟩.
[47] Tisserand M. Progress in the prevention of falls caused by slipping. Ergonomics 1985;28(7):1027–42. https://doi.org/10.1080/00140138508963225.
[48] Tuononen AJ, Kriston A, Persson B. Multiscale physics of rubber-ice friction. J Chem Phys 2016;145(11). https://doi.org/10.1063/1.4962576.
[49] Wåhlin J, Leisinger S, Klein-Paste A. The effect of sodium chloride solution on the hardness of compacted snow. Cold Reg Sci Technol 2014;102:1–7. https://doi.org/10.1016/j.coldregions.2014.02.002.
[50] Yamaguchi T, Hatanaka S, Hokkirigawa K. Effect of step length and walking speed on traction coefficient and slip between shoe sole and walkway. Tribol Online 2008;3(2). https://doi.org/10.2474/trol.3.59.
[51] Yamaguchi T, Hsu J, Li Y, Maki BE. Efficacy of a rubber outsole with a hybrid surface pattern for preventing slips on icy surfaces. Appl Ergon 2015:*51*. https://doi.org/10.1016/j.apergo.2015.04.001.
[52] Yamaguchi T, Katsurashima Y, Hokkirigawa K. Effect of rubber block height and orientation on the coefficients of friction against smooth steel surface lubricated with glycerol solution. Tribol Int 2017:*110*. https://doi.org/10.1016/j.triboint.2017.02.015.
[53] Yamaguchi T, Umetsu T, Ishizuka Y, Kasuga K, Ito T, Ishizawa S, et al. Development of new footwear sole surface pattern for prevention of slip-related falls. Saf Sci 2012;50(4). https://doi.org/10.1016/j.ssci.2011.12.017.